RSC Advances

ROYAL SOCIETY OF CHEMISTRY

www.rsc.org/advances

Journal Name

ARTICLE

Conductive properties and mechanism of different polymers doped by carbon nanotubes/polypyrrole 1 D hybrid nanotubes

Received 00th January 20xx,
Accepted 00th January 20xx

DOI: 10.1039/x0xx00000x

www.rsc.org/

*Hong-xin Tan, Xue-cheng Xu**

We suggested a method to reduce the amount of multi-walled carbon nanotubes (MWNTs) for fabricating polymer composites, and revealed the electron transport mechanism in polymer matrixes with different polarity. Specifically, one-dimension (1 D) hybrid nanotubes (MPPy) have been easily prepared by in-situ polymerization with appropriate ratio of pyrrole to MWNTs. Three matrixes including polyvinyl chloride (PVC), poly (methyl methacrylate) (PMMA) and polystyrene (PS) were separately mechanical blending with MPPy nanotubes. Three families of composites (MPPy/PVC, MPPy/PMMA, MPPy/PS) achieved electrical conductivity higher than 10^{-5} S/cm at 0.3 wt %, 0.8 wt % and 1.5 wt % of MWNTs. The amounts of MWNTs were an order of magnitude lower compared to bare MWNTs used as fillers. The highly ordered chain structure of PPy grown along the surface of MWNTs might be responsible for the good performance of MPPy nanotubes as indicated by FESEM, X-ray photoelectron spectroscopy and Hall Effect Measurement System analysis. We combined doping effect and tunneling distance to explore the conductive mechanism in three matrixes. The more potent doping effect and longer tunneling distance in MPPy/PVC families enabled sharp improvement of carrier concentration and therefore lower percolation threshold, compared to that of MPPy/PMMA and MPPy/PS families.

Introduction

Polymers doped by carbon nanotubes (CNTs) with notably electrical, thermal, and mechanical properties have attracted tremendous attention in both academia and industry.[1-4] Many researchers have centered on improving the dispersion of CNTs, to produce CNTs/polymer composites with high conductivity and low content of CNTs in the past years.[5-7] Besides, finding new CNTs-based multi-component fillers would be a new way to achieve this goal.

Up to now, chemical functionalization methods, such as covalent grafting,[8, 9] doping,[10] and ion beam treatment have been used to improve the intertube contact, but these methods inevitably disturbed the conjugated system of CNTs and thus impair the conductive properties of the resulting composites. Over the past few years, hybrid CNTs fillers with no destruction to conjugated structure of CNTs have been synthesized to fabricate CNTs/polymer composites with reduced consumption amount of CNTs. Multi-branched polyaniline/multi-walled carbon nanotubes (MWCNTs) hybrids,[11] nano-hybrid dopant such as CNTs/PPy nano-composites,[12] CNTs coated with polyaniline[13] has been employed to dope polymer matrixes to obtain high dielectric permittivity and low electrical percolation thresholds. Hybrid fillers of polyethylene containing 15 wt % of MWNTs have been employed to melt mixed with polyethylene matrix, and the composites obtained low percolation threshold at 0.4 vol %.[14] Nevertheless, these hybrid fillers are limited upon application because complex mixed processes (*e.g.* melt blending) were needed to improve the dispersion of CNTs. These hybrid fillers also exhibit good electrical conductivity at the cost of large content of CNTs. Thus, it is necessary to synthesis new hybrid fillers with good conductivity and low content of CNTs in a simple and low-cost way.

The reported electrical conductivities of assembled CNTs/polymer products (*e.g.*, fibers, films) are always much lower than that of the pure CNTs, mainly due to the lack of effective electron transport pathways from tube to tube.[15-17] CNT thin films (assembled large area networks of CNTs) have been reviewed previously with most emphasis on the electrical

[a] *Department of Physics, East China Normal University, 500 Dong Chuan Road, Shanghai 200241, China.*
[b] *Address correspondence to: xcxu@phy.ecnu.edu.cn*

DOI: 10.1039/x0xx00000x

properties of the network and their application in electronics.[18-20] It has been reported that, the conformation and arrangement of polymer chains are critical to the electrical conductivity of CNTs/polymer composites.[21] An expanded chain conformation and an ordered chain arrangement would result in a reduced barrier of both interchain and intrachain hopping, and thus, enhanced electrical conductivity.[22, 23] It is considered to be vital to construct an ordered polymer structure for realizing high electrical performance in conducting polymers.

CNTs are best candidates for 1D templates for generating ordered polymer layers owning to their extremely stable well-defined 1D nanostructure and excellent electric and mechanical properties.[24, 25] Some researchers have utilized self-assembly to obtain ordered polymer chain around the surface of CNTs.[26, 27] CNTs/poly(vinyl acetate),[3] CNTs/poly (3,4-ethlenedioxythiophene) poly(styrenesulfonate) composite films,[28] and CNTs/polyaniline hybrid nanocomposites[21] achieved remarkably enhanced thermoelectric properties, benefiting from their ordered construction of polymers.

Among the best-known conducting polymers, PPy is considered as one of the most promising materials because of its relatively facile processability, good electrical conductivity, environment stability and low price. Moreover, MWNT/PPy hybrides with core-shell structure have been compounded and characterized by a large number of researchers. It has also been reported that π-π interactions existed between the CNT surface and PPy,[29-31] which would benefit the growth of uniform layer along the surface of CNTs. However, the configuration of PPy affected by the presence MWNTs, behind the phenomenon of ordered chain growth, has been largely neglected.

Our work presented the preparation of highly conductive MPPy 1 D hybrid nanotubes by in-situ polymerization and three families of composites by mechanical blending with PVC, PMMA, PS matrixes. The aim of this study was to investigate the change of connecting type in PPy polymerization process as influenced by MWNTs and explore a method to reduce the amount of MWNTs in the derived nanocomposites. In addition, the effect of tunnelling distance and doping effect on carrier concentration, carrier mobility and conductivity have been evaluated.

2. Experimental Section

2.1 Preparation of PPy, MPPy

The nanocomposites were synthesized by one-step in situ polymerization of Pyrrole in the presence of MWNTs with ammonium peroxidisulfate (APS) as the oxidant. Pyrrole monomer (98%, Sinopharm Chemical Reagent Co.,Ltd.) was purified by distillation under reduced pressure. The MWNTs (95%, Chengdu Organic Chemicals Co., Ltd.) were 20-30 nm in diameter and 5-15 μm in length. A solution of 100 mL of 1 mol/L HCl containing different masses of MWNTs (0, 0.045, 0.220, 0.450, and 0.714 g) was kept sonication for 30 minutes, Another 20 minutes of sonication was needed after adding pyrrole monomer (4.19 mL) into the solution and then transferred to three-necked, round-bottomed flask under ice bath, The 30 mL HCl solution containing APS (1.53 g, keeping the molar ratio of pyrrole 1:1) was slowly added dropwise into the suspension with constant magnetic stirring. After an additional 4h reaction, the mixture was filtered and the residue was washed thoroughly with deionized water and ethanol. The cleaning procedure above was repeated three times. The obtained black powders were dried at 40 ℃under vacuum for at least 24 h. The resulting composites were named PPy, $MPPy_1$, $MPPy_5$, $MPPy_{10}$ and $MPPy_{15}$ orderly.

2.2 Polymer doping

The $MPPy_{10}$ and $MPPy_{15}$ hybrids were separately blended into the PVC (Shanghai Aladdin Chemical Co.), PMMA and PS powders by grinding them together in an agate mortar. PMMA and PS powders were synthesis in our laboratory according to the previous study.[32, 33] The hybrid powders were pressed into wafer-shaped samples and ground in the agate mortar again. This procedure was repeated three times. After fully blended, these samples were pressed into wafers with a thickness of 2 mm and a diameter of 13 mm at a constant pressure of 20 MPa, with pressure holding time of 1 min.

2.3 Characterization

The resistance (R) of each composite was measured by using a DC kelvin bridge and a standard four-probe technique at room temperature, and then the DC electric conductivity (σ_{DC}) of the composite was calculated from the relationship $\sigma_{DC} = \mathrm{L}/RS$, where L and S are the thickness and sectional area of the composites, respectively. The carrier concentration and carrier mobility was measured by a Hall Effect measurement instrument (HM2000) at room temperature. The chemical structure and property of the composites were analyzed by X-ray Photoelectron Spectroscopy (Perkin-Elmer PHI 5000C ESCA System) using non-mono chromatized Mg-Kα radiation for excitation. The Field emission scanning electron microscopy (FESEM) imaging was performed with a JSM6700F (JEOL) field emission scanning electron microscope. Dielectric properties were measured on a broadband dielectrics spectrometer (Novocontrol Concept 80, Hundsangen, Germany) at room temperature over a frequency ranging from 10^4 to 10^5 Hz.

3. Results and discussion

3.1 MPPy hybrid nanotubes

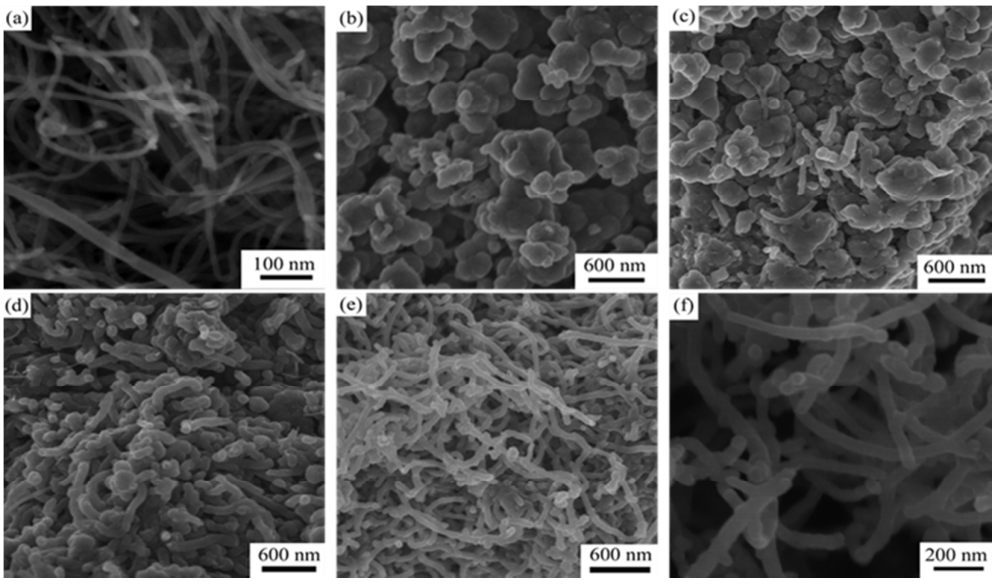

Figure 1. FESEM images of MWNTs (a), $MPPy_1$ (MWNTs 1 wt %/PPy) (b), $MPPy_5$ (MWNTs 5wt %/PPy) (c), $MPPy_{10}$ (MWNTs 10 wt % / PPy) (d) and $MPPy_{15}$ (MWNTs 15 wt %/PPy) (e). (f) is the image of $MPPy_{15}$ (MWNTs 15 wt %/PPy) with a greater magnification.

Figure 1 (a) shows the microstructures of pure MWNTs. The outer diameter of MWNTs is about 25-30 nm. (b) (c) (d) (e) show microstructures of $MPPy_1$, $MPPy_5$, $MPPy_{10}$ and $MPPy_{15}$ at the same magnification. (f) is the amplification of (e), shows the tubular structure of $MPPy_{15}$ more syllabify. As shown in (b) and (c), $MPPy_1$ and $MPPy_5$ consist of micrometer-sized spherical particles and no tubular structure can be found. However, the bulk morphology of $MPPy_{10}$ changes from granular particulates to a mat of 1 D nanotubes with an average diameter of 60-65 nm (see Figure 1 (d)). $MPPy_{15}$ exhibited a more defined tubular structure at the same magnification, as shown in (e). This idealized uniform tubular structure of $MPPy_{15}$ could be observed clearly in Figure 1 (f) with a greater magnification. These results indicated that, MWNTs acted as templates for the polymerization of Py molecules to form homogeneous layers.

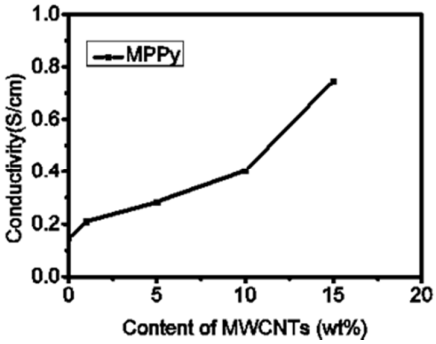

Figure 2. Electrical conductivity of MPPy with different MWNTs contents.

The electrical conductivity of the MPPy complex starts with a flat increase and tends to rising sharply from 10 wt% to 15 wt% (see Figure 2). The enhancement of conductivity of MPPy may come from two parts: one is mainly attributed to the incorporation of MWNTs, the other may come from the ordered chain packing of PPy, which was confirmed as follow by XPS. Accordingly, the phase when 1 D tuber structures have formed (10 wt % to 15 wt % of MWNTs) show a more precipitous rise in conductivity compared with a relative mild increase when MWNTs content started from 0 wt % to 10 wt %.

Previous studies indicated that there was π-π interaction between MWNTs and PPy in MWNTs/PPy composites.[30, 34] This interaction was confirmed more clearly in the 1 D MPPy hybrid nanotubes by XPS results. The main peak of C1s spectrum of pure PPy was located at 285.83 eV, but it shifted down to 285.44 eV upon doped by MWNTs, which indicated that the conjugated system of PPy layer was affected by the π-electron of MWNTs. This interaction may be favorable for the uniform coating of PPy on the surface of MWNTs.

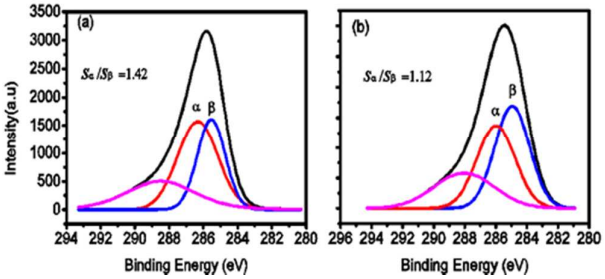

Figure 3. C 1s spectra of the samples (a) PPy (b) $MPPy_{15}$, α and β peaks represent the α type and β type of carbon atoms of Pyrrole monomer.[25, 35]

In order to explore the configuration of PPy layer, we fitted PPy spectrum with three chemical components (Figure 3). These two peaks with lower electron binding energies corresponding to α and β type of carbon atoms of Pyrrole monomer.[25, 35] The wider peaks located at 288.3 eV probably came from the disordered carbon structures (e.g., C at terminal groups) in Pyrrole rings. The area of α-C and β-C in Figure 3 represent contents of carbon atoms with C-H bond

Journal Name

ARTICLE

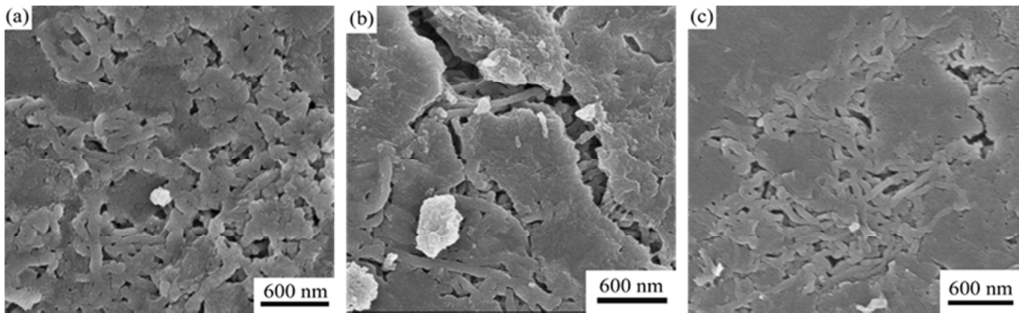

Figure 4. FESEM images of (a) MPPy/PS, (b) MPPy/PMMA and (c) MPPy/PVC composites with 10 wt % of $MPPy_{15}$.

which not have participated the construction of polymer chains. In $MPPy_{15}$, the ratio of S_α/S_β was reduced 0.3 with respect to pure PPy. The content of α-C with C-H bond decreased means that, more α-C have participated the construction of polymer chains. So, Py monomers were induced to connect in α-α order in presence of MWNTs. This order significantly promoted a more planar configuration of PPy, which would in favor of electrical transport between PPy and MWNT, and guaranteed high electrical conductivity of 1 D $MPPy_{10}$ and $MPPy_{15}$ hybrid nanotubes.

3.2 MPPy reinforcement of polymers

The dispersions of MPPy nanotubes into the polymer matrixes were evaluated by FESEM (see Figure 4 (a)-(c) with 10 wt % $MPPy_{15}$ nanotubes in three matrixes). We could see similar dispersion of $MPPy_{15}$ hybrid nanotubes in (a) (b) and (c). So the dispersion of $MPPy_{15}$ nanotubes is not the main factor to impact the distinct electrical conductivity of composites.

The electrical conductivity over the three families of composites (PS, PMMA and PVC were used as matrixes) is plotted in Figure 5, as a function of MWNTs content. $MPPy_{10}$ and $MPPy_{15}$ hybrid nanotubes were respectively used as fillers in (a) and (b). In $MPPy_{10}$/polymer composites, the electrical percolation thresholds appeared at 0.3 wt %, 0.8 wt %, 1.5 wt % respectively in PVC, PMMA, PS matrixes. Three curves in Figure 5 (b) keep similar trend and percolation thresholds, but $MPPy_{15}$/polymer composites process better conductivity at their corresponding percolation thresholds. This could be attributed to the better tubular structure of $MPPy_{15}$, as shown in Figure 1. In contrast, the electrical percolation thresholds of MWNTs/polymer composites appeared at 5 wt%, 10 wt%, 10 wt% in PVC, PMMA, PS matrixes, respectively (Figure 5 (c)). Apparently, the dosage of MWNTs can be greatly reduced with an order of magnitude when using MPPy hybrid nanotubes as fillers instead.

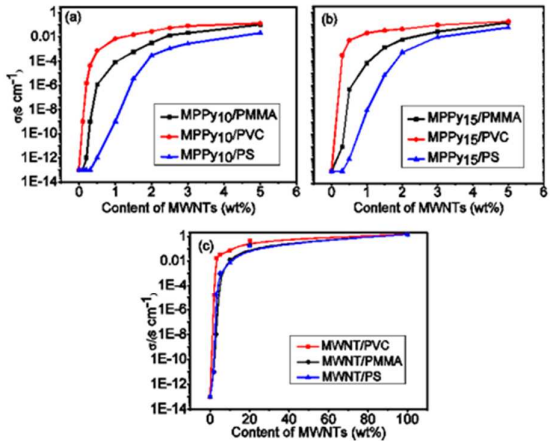

Figure 5. Electrical conductivity of composites based on PS, PMMA and PVC matrixes versus mass fraction of MWNTs, (a) (b) and (c) were $MPPy_{10}$, $MPPy_{15}$ and MWNTs used as fillers, respectively.

Three curves in Figure 6 (a) and (b), corresponding to $MPPy_{15}$/PS, $MPPy_{15}$/PMMA and $MPPy_{15}$/PVC composites, represent the carrier concentration and mobility of composites with different mass fractions of $MPPy_{15}$. All three curves of carrier concentration possess two phases: first a sharp increase and then turn to a platform. Obviously, three families of composites reach their inflexion with different speeds: a sharp increase of carrier concentration with 8 orders of magnitude in PVC matrix when the doping content was only 5%. While, in PMMA and PS matrixes, the carrier concentration finish their first phase of increase later at 10% and 20% doping contents. After the doping content exceed their inflexions, the carrier concentration almost unchanged, but their carrier mobility start to increase (see Figure 6(b)). With the doping content increased to 30%, the carrier mobility

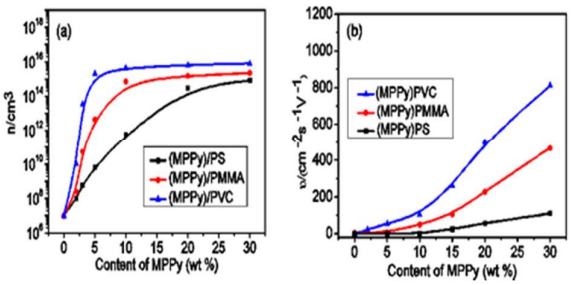

Figure 6. Relationship between carrier concentration and $MPPy_{15}$ mass fraction (a), carrier mobility and $MPPy_{15}$ mass fraction (b) of samples.

in PS, PMMA, PVC matrixes reached 109.6, 466.3, 810.1 $cm^{-2}s^{-1}V^{-1}$, respectively.

The dielectric permittivity of composites had discrepant trends with doping content of $MPPy_{15}$ hybrid (see Figure 7). In PVC matrix, with a small addition of $MPPy_{15}$ nanotubes, dielectric permittivity of the resultant composites has sharply increased，different from that in PS and PMMA matrixes with relatively languid uptrends. Specifically, the dielectric permittivity at 10^2 Hz of $MPPy_{15}$/PVC composite has already reached 504 with 10% content of $MPPy_{15}$ hybrid, while, the dielectric consistent of $MPPy_{10}$/PMMA and $MPPy_{10}$/PS were merely 23.8 and 5.06. The dielectric properties of three families are consistent with electrical conductivity.

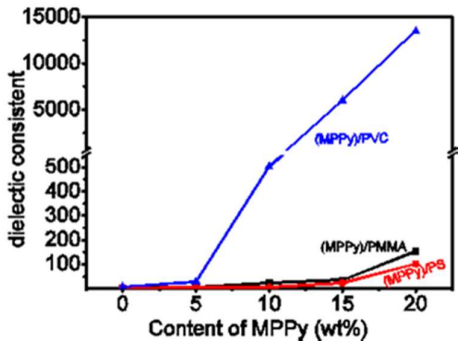

Figure 7. Relationship between dielectric permittivity of composites and mass fraction of MPPy15 hybrid nanotubes.

3.3 Interaction between MPPy and matrixes

As above-mentioned results demonstrated, matrixes with different polarity resulted in discrepant percolation thresholds. To investigate the influence of interaction between MPPy hybrid nanotubes and matrixes on the electrical percolation thresholds, we compares the C1s spectra of pure matrixes with resultant composites [w ($MPPy_{15}$ hybrid nanotubes) = 30%] (see Figure 8 (a), (b) and (c)). Table 2 lists the shift of main peak position distinctly. The main peaks of resultant composites move to the direction of lower binding energy relative to the pure matrixes except for $MPPy_{15}$/PS composite, which shifted to the opposite direction. The range of main peak shift is also different: in $MPPy_{15}$/PVC composites a remarkable shift of main peak with 0.9 eV compared with $MPPy_{15}$/PMMA composites with a moderate shift of 0.4 eV and a weak shift in $MPPy_{15}$/PS composites with 0.15 eV. Larger shifts may imply relatively higher degrees of doping effect. Regarding the interaction between PS and $MPPy_{15}$ hybrid nanotubes, the phenyl group acted as electron-donator to the hybrid nanotube, which is consistent with Samarajeewa's research.[36] PMMA and PVC possess stronger electronegativity with the ester group and chlorine group respectively, leading to the π electron cloud shift to matrixes, so a down shift of the binding energy in $MPPy_{15}$/PMMA and $MPPy_{15}$/PVC composites. The XPS results indicate that the level of doping effect between MPPy hybrid nanotubes and matrixes were varies from matrixes with different polarity.

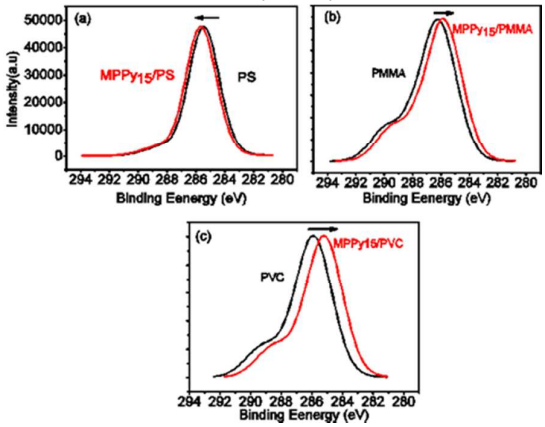

Figure 8. C1s spectra of the pure matrixes and resultant composites with 30 wt% of $MPPy_{15}$ hybrid nanotubes.

Table 2. The main peak position of the samples

matrix	BE (eV) （w%= 0%）	BE (eV) （w%= 30%）	ΔBE (eV)
PS	285.5	285.65	0.15
PMMA	286.2	285.80	-0.4
PVC	286.0	285.10	-0.9

3.4 Conductive mechanism analysis

As stated above, our work reported herein has two targets: one is preparing highly conductive MPPy/polymer composites with reduced amount of MWNTs, and the other is revealing the origin of the different percolation thresholds in three matrixes. Taking all results into consideration, including the structure and properties of hybrid nanotubes, doping effect and discrepant percolation thresholds, we deduced the whole conductive mechanism in Figure 9.

MPPy hybrid nanotubes with 1 D conjugate tubular structure were prepared by in-situ polymerization (Figure 9 a-b). This expanded chain conformation and the highly ordered PPy layer endowed the hybrid nanotubes with high electrical property. Mechanical blending of MPPy hybrid nanotubes and matrixes (PS, PMMA and PVC) yielded three families of composites (c, d and e). The content of MWNTs to reach percolation threshold was an order of magnitude lower compared with that of MWNTs/polymers composites. In addition, three matrixes with different polarity, obtained variant percolation thresholds.

Journal Name

ARTICLE

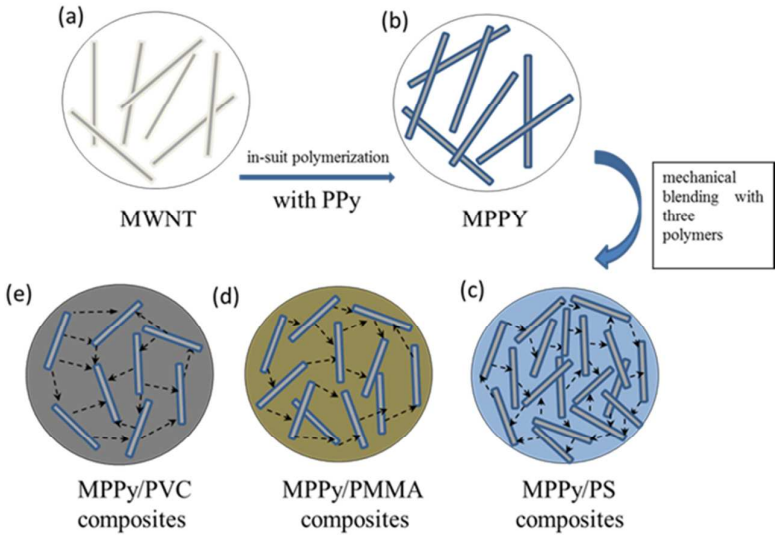

Figure 9. The conductive mechanism for different polymer composites in the entire fabrication process.

Kyrylyuk and coworker [37] reported that tunneling distance could be estimated based on the time-independent Schrodinger equation:

$$\xi = \frac{\hbar}{\sqrt{m_e(E_e - E_f)}} \quad (1)$$

$$E_e = \frac{k_B T l_B}{2\Lambda} \quad (2)$$

Where, $\hbar$ is the reduced Planck constant, m_e is the electron mass, E_f and E_e are the energies of a conduction electron on a tube and in the matrixes. For E_f and E_e, we presume the estimated Fermi energy of an electron on a bare MPPy hybrid nanotube and the Born energy of an electron in a matrix to be the relevant energy scale.[37] The equation of Born energy is given in Equation (2) , with l_B the Bjerrum length which is inverse of the dielectric constant of the polymer matrix and Λ the thermal wavelength of the spatially delocalized electron in the matrixes.[38]

For the three matrixes PS, PMMA, PVC, the relative dielectric permittivities are 3.3, 4.5 and 7.8, respectively. The calculated Born energies of the pure matrixes are: E_{PVC} = 0.288 eV, E_{PMMA} = 0.5 eV, E_{PS} = 0.68 eV. Due to same MPPy nanotubes were used as fillers, E_f keeps a constant value in three families of composites. So the tunneling distances keep the order: $\xi_{PVC} > \xi_{PMMA} > \xi_{PS}$. On the other hand, the doping effect represents the interaction between MPPy hybrid nanotube and matrix, which did favor to the connectedness of MPPy hybrid nanotubes. The XPS results manifest the doping effect of MPPy/PVC families was stronger than that of MPPy/PMMA families and MPPy/PS families.

Combining the tunneling distances and doping effect, we could sum up, in PVC matrix with a few percentages doping of 3 wt % MPPy nanotubes, the distance between two nanotubes has reached the tunneling distance, and the strong doping effect enabled a global connection of MPPy nanotubes (see Figure 9 (e)). So the carrier concentration was largely improved with 8 orders of magnitude and the electrical percolation threshold appeared. MPPy/PMMA and MPPy/PS families with short tunneling distances and poor doping effects, the $MPPy_{15}$ hybrid nanotubes in PMMA and PS matrixes were connected at more intensive scale (see Figure 9 (d) and (c)), which resulted in gentle increase of carrier concentration and higher percolation thresholds. After the doping contents pass their percolation thresholds, all the MPPy nanotubes in three matrixes have connected and the conductive networks have formed, so platforms of the carrier concentration appear in three families and the carrier mobility begin to rise. The level of doping effect affects the increment of the carrier mobility and therefore the electrical conductivity in the second phase.

The situation changed when it came to MWNTs/polymer system, the percolation thresholds of three matrixes didn't show such obvious difference, as shown in Figure 5 (c). This may attribute to poor doping effect between MWNTs and three matrixes. The connectedness criterions of MWNTs nanotubes in three matrixes were similar. So these three curves corresponding to electrical conductivity of three families coincided when MWNTs used as fillers.

4. Conclusion

A study associated with 1 D MPPy hybrid nanotubes and electrical properties of derived nanocomposites was carried out in this work. MWNTs acted as 1 D hard template for generating ordered PPy layer, as confirmed by SEM and XPS results. A more planar configuration of PPy influenced by MWNTs may be in favor of good performance of MPPy in electrical conductivity. The amount of MWNTs needed to reach the threshold could be reduced by an order of magnitude but the resulting composites exhibited similar electrical conductivity, compared to using MWNTs as fillers. This finding implies that highly ordered hybrid nanotubes with low content of MWNTs could be used as fillers to reduce the consumption of MWNTs.

Doping effects and tunneling distance were combined to clarify the diversity of percolation threshold in three matrixes. It may useful to develop highly conductive CNTs/polymer composites by an optimized choice of matrix with higher dielectric permittivity and stronger doping effect with fillers.

Acknowledgements

The authors thank East China Normal University for financial support. The authors also thank Zhao-yang Zhang for technical support.

Notes and references

1 T. Sekitani, Y. Noguchi, K. Hata, T. Fukushima, T. Aida, T. Someya, *Science.,* 2008, **321**, 1468-1472.
2 L. Larrimore, S. Nad, X. Zhou, H. Abruna, P. L. McEuen, *Nano Lett.,* 2006, **6**, 1329-1333.
3 C. Yu, Y. S. Kim, D. Kim, J. C. Grunlan, *Nano Lett.,* 2008, **8**, 4428-4432.
4 M. M. Hamedi, A. Hajian, A. B. Fall, K. Hakansson, M. Salajkova, F. Lundell, L. Wagberg, L. A. Berglund, *ACS Nano,* 2014, **8**, 2467-2476.
5 T. McNally, P. Potschke, P. Halley, M. Murphy, D. Martin, S. E. J. Bell, G. P. Brennan, D. Bein, P. Lemoine, J. P. Quinn, *Polymer,* 2005, **46**, 8222-8232.
6 O. Breuer, U. Sundararaj, *Polym. Compos.,* 2004, **25**, 630-645.
7 J. K. W. Sandler, J. E. Kirk, I. A. Kinloch, M. S. P. Shaffer, A. H. Windle, *Polymer,* 2003, **44**, 5893-5899.
8 J. Zhu, B. S. Shim, M. Di Prima, N. A. *J.* Kotov, *Am. Chem. Soc.,* 2011, **133**, 7450-7460.
9 S. N. Kourkouli, A. Siokou, A. A. Stefopoulos, F. Ravani, T. Plocke, M. Müller, J. Maultzsch, C. Thomsen, K. Papagelis, J. K. Kallitsis, *Macromolecules,* 2013, **46**, 2590-2598.
10 Y. Zhao, J. Wei, R. Vajtai, P. M. Ajayan, E. V. Barrera, *Sci. Rep.,* 2011, **10**, 1038-1052.
11 Z. Qiang, G. Liang, A. Gu, L. Yuan, *Compos. Part A,* 2014, **64**, 1-10.
12 B. Yu, X. Xu, *RSC Adv.,* 2014, **10**, 2-8.
13 T. Zhou, J.-W. Zha, Y. Hou, D. Wang, J. Zhao, Z.-M. Dang, *ACS Appl. Mater. Interf.,* 2011, **3**, 4557-4560.
14 M. Jouni, J. Faure-Vincent, P. Fedorko, D. Djurado, G. Boiteux, V. Massardier, *Carbon,* 2014, **76**, 10-18.
15 M. A. Topinka, M. W. Rowell, D. Goldhaber-Gordon, M. D. McGehee, D. S. Hecht, G. Gruner, *Nano Lett.,* 2009, **9**, 1866- 1871.
16 L. Hu, D. S. Hecht, G. Gruener, *Chem. Rev.,* 2010, **110**, 5790-5844.
17 P. N. Nirmalraj, P. E. Lyons, S. De, J. N. Coleman, J. J. Boland, *Nano Lett.,* 2009, **9**, 3890-3895.
18 C. M. Jiang, A. Saha, C. C. Young, D. P. Hashim, C. E. Ramirez, P. M. Ajayan, M. Pasquali, A. A. Marti, *ACS nano,* 2014, **8**, 9107-9112.
19 C. Jiang, A. Saha, C. Xiang, C. C. Young, J. M. Tour, M. Pasquali, A. A. Marti, *ACS nano,* 2013, **7**, 4503-4510.
20 A. Saha, C. Jiang, A. A. Marti, *Carbon,* 2014, **79**, 1-18.
21 Q. Yao, L. Chen, W. Zhang, S. Liu, X. Chen, *ACS Nano,* 2010, **4**, 2445–2451.
22 Q. Yao, L. D. Chen, X. C. Xu, C. F. Wang, *Chem. Lett.,* 2005, **34**, 522-523.
23 Y. Hiroshige, M. Ookawa, N. Toshima, *Synth. Met.,* 2006, **156**, 1341-1347.
24 Y. Zhang, H. J. Dai, *Appl.Phys. Lett.,* 2000, 77, 3015-3017.
25 P. M. Ajayan, O. Stephan, P. Redlich, C. Colliex, *Nature,* 1995, **375**, 564-567.
26 M. J. O'Connell, P. Boul, L. M. Ericson, C. Huffman, Y. H. Wang, E. Haroz, C. Kuper, J. Tour, K. D. Ausman, R. E. Smalley, *Chem. Phys. Lett.,* 2001, **342**, 265-271.
27 F. Balavoine, P. Schultz, C. Richard, V. Mallouh, T. W. Ebbesen, C. Mioskowski, *Angew. Chem. Int. Edit.,* 1999, **38**, 1912-1915.
28 D. Kim, Y. Kim, K. Choi, J. C. Grunlan, C. Yu, *ACS Nano,* 2010, **4**, 513-523.
29 J. Liu, H.-Q. *J.* Yu, *Electron. Mater,* 2014, **43**, 1181-1187.
30 Y. Yu, C. Ouyang, Y. Gao, Z. Si, W. Chen, Z. Wang, G. *J.* Xue, *Polym. Sci. Part A: Polym. Chem.,* 2005, **43**, 6105-6115.
31 C. Bin, L. Jun, L. Delzeit, P. Qibing, *Proc. SPIE - Int. Soc. Opt. Eng.,* 2007, **6423**,1-8.
32 J.-M. Thomassin, M. Trifkovic, W. Alkarmo,C. Detrembleur, C. Jérôme, C. Macosko, *Macromolecules,* 2014, **47**, 2149-2155.
33 R. Xu, X. Xu. *RSC Advances,* 2014, 79, 42226-42233.
34 N. G. Sahoo, Y. C. Jung, H. H. So, J. W. Cho, *Synth. Met.,* 2007, **157**, 374-379.
35 R. D. Sherman, L. M. Middleman, S. M. Jacobs, *Polym. Eng. Sci.,* 1983, **23**, 36-46.
36 D. R. Samarajeewa, G. R. Dieckmann, S. O. Nielsen, I. H. Musselman, *Carbon,* 2013, **57**, 88-98.
37 A. V. Kyrylyuk, P. *P.* van der Schoot, *Natl. Acad. Sci. USA,* 2008, **105**, 8221-8226.
38 J. N. Israelachvili, *Intermolecular and Surface Forces*, Academic: London 1985.